



HAL
open science

Flow-fiber coupled viscosity in injection molding simulations of short fiber reinforced thermoplastics

Tianyi Li, Jean-François Luyé

► **To cite this version:**

Tianyi Li, Jean-François Luyé. Flow-fiber coupled viscosity in injection molding simulations of short fiber reinforced thermoplastics. *International Polymer Processing*, 2018. hal-01683052v2

HAL Id: hal-01683052

<https://hal.science/hal-01683052v2>

Submitted on 11 Mar 2018 (v2), last revised 15 Sep 2023 (v5)

HAL is a multi-disciplinary open access archive for the deposit and dissemination of scientific research documents, whether they are published or not. The documents may come from teaching and research institutions in France or abroad, or from public or private research centers.

L'archive ouverte pluridisciplinaire **HAL**, est destinée au dépôt et à la diffusion de documents scientifiques de niveau recherche, publiés ou non, émanant des établissements d'enseignement et de recherche français ou étrangers, des laboratoires publics ou privés.

Flow-fiber coupled viscosity in injection molding simulations of short fiber reinforced thermoplastics

Tianyi Li^{a,*}, Jean-François Luyé^a

^aPromold, 43 rue Boursault, 75017 Paris, France

Abstract

The main objective of this communication is to numerically investigate the use of fiber-dependent viscosity models in injection molding simulations of short fiber reinforced thermoplastics with a latest commercial software (Moldflow Insight 2018). We propose to use the homogenization-based anisotropic rheological model to take into account possible flow-fiber coupling effects. The original model is adapted and then implemented in the Moldflow Insight API framework. Numerical simulations are performed in a test-case rectangle flat plate geometry with two latest fiber orientation models. The resulting coupled flow kinematics and fiber evolutions are then compared to the standard uncoupled simulations. Interpretations are given based on detailed post-processing of the field results. Certain deformation conditions are expected to be better taken into account, which may also in return lead to an improved fiber orientation prediction.

Keywords: Injection molding, Fibers, Rheological properties, Process Simulation

1. Introduction

Short fiber reinforced thermoplastics are gaining popularity in industries because they can guarantee mechanical resistance specifications while achieving overall part weight reductions. Integrative simulation procedures [Adam and Assaker \(2014\)](#) are extremely appealing since heterogeneous local microstructure information caused by different processing steps can then be transferred to the subsequent mechanical simulations. In particular, fiber-induced material anisotropy wisely placed in some critical loaded regions can be better taken into account, resulting in an even optimized part design.

An experimentally validated injection molding simulation constitutes hence the cornerstone of these integrated simulations of injected short fiber reinforced thermoplastics. It is now well known that an inaccurate prediction of fiber orientation distribution in the part could affect ultimate structural response simulations via finite element analyses, see [Wedgewood et al. \(2017\)](#). According to [Rolland et al. \(2016\)](#), a well predicted injection molding induced skin-shell-core fiber orientation structure (cf. [Papathanasiou \(1997\)](#) for a comprehensive review on this subject) is also crucial since it contributes to a correct prediction of damaging mechanism and ultimate failure of these composites.

It is discovered that the fiber orientation models currently available in commercial softwares produce often unsatisfactory predictions in the core region, see [Kleindel et al. \(2015\)](#); [Tseng et al. \(2017\)](#). Compared to experimental results, fibers are estimated to be over-aligned in the flow direction on the mid-surface and the width of the core is also under predicted. Since the core region is in general dominated by extensional

*Corresponding author

Email addresses: tianyi.li@promold.fr (Tianyi Li), jfluye@promold.fr (Jean-François Luyé)

flows transverse to the filling direction, it can be argued that these elongational deformations are not correctly taken into account in current models and a flow-fiber coupled simulation with fiber-dependent rheological properties may be more appropriate, cf. [Tucker \(1991\)](#); [Jørgensen et al. \(2017\)](#).

There exists already a relatively abundant literature on different flow-induced rheological models, see [Phan-Thien and Zheng \(1997\)](#) for instance for a quick review. The basic idea is that under shear flows fibers contribute less to the overall suspension viscosity when they are aligned to the shear direction, while it is the opposite for elongational flows in the same direction, cf. [Laun \(1984\)](#). Since, these fiber-dependent viscosity models have been applied to flow and injection molding simulations, see for instance [Ranganathan and Advani \(1993\)](#); [Verweyst and Tucker \(2002\)](#); [Vincent et al. \(2005\)](#); [Redjeb et al. \(2006\)](#); [Mazahir et al. \(2013\)](#); [Costa et al. \(2015\)](#); [Tseng et al. \(2017\)](#). The research is still on-going and no definite conclusions have been yet reached on whether or not these flow-fiber coupling effects are really important for most cases. That's probably one of the reasons why currently almost all commercial injection molding softwares still perform an uncoupled analysis.

The objective of this paper is thus to present some updated results on the subject with a latest injection molding software (Moldflow Insight 2018). Thanks to its API framework [Costa et al. \(2015\)](#), in [Section 2](#) a representative anisotropic fiber-induced viscosity model is implemented as a user-defined viscosity function. In particular, fiber orientation is explicitly taken into account in the viscosity. Compared to some previous researches, in [Section 3](#) the flow-fiber coupling effects are numerically evaluated by using more physical injection conditions via non-isothermal three-dimensional finite element computations. Furthermore two latest experimentally validated fiber orientation models (RSC and MRD) are also compared in terms of their possible different contributions to the overall coupling. Conclusions and future research directions drawn from the numerical results are indicated in [Section 4](#).

General notation conventions adopted in this paper are summarized as follows. Scalar-valued quantities will be denoted by italic Roman or Greek letters like temperature T and pressure p . Vectors and second-order tensors as well as their matrix representation will be represented by boldface letters. This concerns for example the 2nd-order fiber orientation tensor \mathbf{a} , the stress tensor $\boldsymbol{\sigma}$ and the rate of deformation tensor \mathbf{D} . Higher order tensors will be indicated by blackboard letters such as the 4th-order orientation tensor \mathbb{A} and the 4th-order viscosity tensor \mathbb{V} . Tensors are considered as linear operators and intrinsic notation is adopted. If the resulting quantity is not a scalar, the contraction operation will be written without dots, such as $(\mathbb{V}\mathbf{D})_{ij} = \mathbb{V}_{ijkl}\mathbf{D}_{kl}$. Inner products (full contraction giving a scalar result) between two tensors of the same order will be denoted with a dot, such as $\mathbf{D} \cdot \mathbb{V}\mathbf{D} = \mathbb{V}_{ijkl}\mathbf{D}_{kl}\mathbf{D}_{ij}$. The Einstein summation convention is assumed.

2. Flow-fiber coupled viscosity models

2.1. Anisotropic fiber-induced rheological equations

For (short) fiber reinforced thermoplastics (that is, when the immersed particle aspect ratio r is sufficiently large, say $r > 20$, which is generally satisfied by fibers), the anisotropy induced by these fibers on the overall suspension rheological properties can be described by the following expression of the stress tensor

$$\boldsymbol{\sigma} = -p\mathbf{I} + 2\eta\mathbf{D} + 2\eta N_p \mathbb{A}\mathbf{D}, \quad (1)$$

where $\boldsymbol{\sigma}$ is the (macroscopic) stress tensor for the fiber reinforced suspension, p is the pressure, \mathbf{I} is the 2nd order identity tensor, $\mathbf{D} = \frac{1}{2} \text{dev}(\nabla\mathbf{v} + \nabla^T\mathbf{v})$ is the deviatoric deformation rate tensor, η refers to the viscosity of the matrix (without fibers) and \mathbb{A} designates the 4th order fiber orientation tensor introduced in [Advani](#)

and Tucker (1987). The interested reader can find detailed theoretic explanation of (1) and homogenization-based derivation of similar models in Lipscomb et al. (1988); Tucker (1991); Phan-Thien and Zheng (1997) and references therein. Note that according to (1), the viscosity of the suspension is now no longer a scalar but a 4th order tensor reflecting the anisotropy induced by fibers

$$\boldsymbol{\sigma} = -p\mathbf{I} + 2\mathbb{V}\mathbf{D} \quad \text{with} \quad \mathbb{V} = \eta(\mathbb{I} + N_p\mathbb{A}), \quad (2)$$

with \mathbb{I} the 4th order identity operator.

In (1) and (2), the coefficient N_p measures the scalar intensity of the anisotropic contribution of fibers to the overall viscosity. In particular when one sets $N_p = 0$, we retrieve the uncoupled scalar viscosity model, completely independent of fiber evolutions during the injection process. Since traditional linear dependence of N_p on volume fraction may not be suitable for concentrated fiber-reinforced suspensions, see Jørgensen et al. (2017), in this communication we adopt the nonlinear functional dependence of N_p on fiber aspect ratio and volume fraction proposed by Phan-Thien and Graham (1991). Its dependence on mass fraction is illustrated in Fig. 1 for a typical 50%wt fiber filled polyamide (Zytel PLS95G50DH2 BK261) with the fitting parameter $A = 50\%$. For comparison, the dilute theory of Ericksen (1959) is also indicated. These two theories agree for small fiber volume concentrations, however for the current case (50%wt), Phan-Thien and Graham (1991)'s model predicts a much larger anisotropic contribution coefficient N_p .

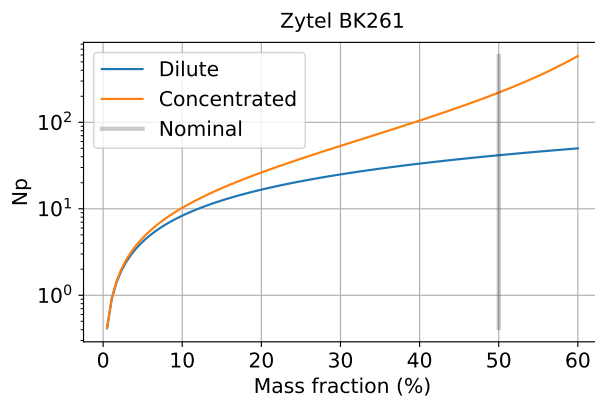


Figure 1: Anisotropic contribution coefficient N_p as a function of volume fraction using Ericksen (1959)'s dilute and Phan-Thien and Graham (1991)'s concentrated theories.

2.2. Optimal scalar approximation of the 4th-order viscosity tensor

In order to evaluate numerically the anisotropic fiber-induced viscosity model in injection molding simulations, we propose to implement (2) in the Moldflow Insight API framework described in Costa et al. (2015).

Currently, only a *scalar* user-defined viscosity function is supported via this interface. Hence, the original model as shown in (2) needs to be adapted for implementation. One novelty of this communication consists in proposing an *optimal* approximate scalar (isotropic) viscosity value of the anisotropic 4th order model.

According to (2), for stress computations the viscosity tensor \mathbb{V} is used via its action $\mathbb{V}\mathbf{D}$ on the current deformation rate tensor \mathbf{D} . The idea is thus to define an effective scalar viscosity value η_* such that the scalar multiplication $\eta_*\mathbf{D}$ is as close as possible to $\mathbb{V}\mathbf{D}$ in a certain sense. In this paper, we simply use the

classical Frobenius norm (square root of the sum of its components) for 2nd order tensors and we minimize the following approximation error

$$\|\eta_* \mathbf{D} - \mathbb{V} \mathbf{D}\|^2 = \min_{\nu} \|\nu \mathbf{D} - \mathbb{V} \mathbf{D}\|^2. \quad (3)$$

Through the Frobenius (elementwise) inner product, the scalar η_* can be simply regarded as the projection of \mathbb{V} in the direction of \mathbf{D} . By a direct calculation of (3), we obtain thus the optimal scalar viscosity approximating the 4th-order anisotropic viscosity when $\mathbf{D} \neq \mathbf{0}$

$$\eta_* = (1 + N_p a_*) \eta \quad \text{with} \quad a_* = \frac{\mathbf{D} \cdot \mathbb{A} \mathbf{D}}{\|\mathbf{D}\|^2} = \frac{\text{tr}(\mathbf{D}^T \mathbb{A} \mathbf{D})}{\|\mathbf{D}\|^2}, \quad (4)$$

where tr is the trace operator for 2nd-order tensors. In (4), the scalar a_* can also be regarded as the optimal equivalent scalar of the 4th order orientation tensor \mathbb{A} , for the current deformation rate tensor \mathbf{D} considered. For $\mathbf{D} = \mathbf{0}$, we can simply set $a_* = 0$.

The computation of this optimal scalar viscosity through (4) requires the 4th order fiber orientation tensor \mathbb{A} . In general in injection molding simulations it can only be recovered approximately from the 2nd order tensor via a particular closure formulation. For consistency, we use the same orthotropic (ORT) closure model described in [Verweyst \(1998\)](#) which is used by default in Moldflow since the version 2017R2. The tensor \mathbb{A} is positive semi-definite by definition, see [Advani and Tucker \(1987\)](#). Accordingly the scalar a_* is non-negative and the optimal scalar suspension viscosity η_* remains equal to or greater than the matrix viscosity η . It is desired that closure formulation also satisfy this property. In [Fig. 2](#), the smallest eigenvalue of \mathbb{A} approximated by the ORT closure is numerically computed for all possible 2nd-order tensor orientations with (a_1, a_2) the two largest eigenvalues of \mathbf{a} , in the TUB triangular domain of [Cintra Jr and Tucker \(1995\)](#). It can be seen that the ORT-approximated \mathbb{A} only loses definite-positiveness for planar or unidirectional orientation states (degenerate cases of 3d orientation states). The semi-positiveness of the ORT model is thus numerically verified.

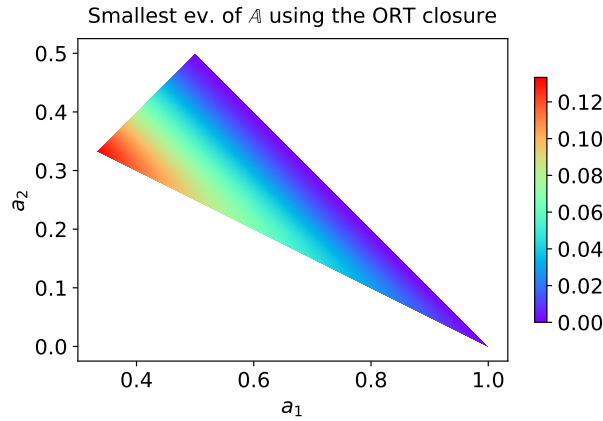


Figure 2: Smallest eigenvalue of the 4th-order fiber orientation tensor approximated by the orthotropic closure formulation in the TUB orientation space.

In order to better understand the optimal scalar viscosity model (4), its behavior under two typical flows (simple shear and planar elongation) frequently present in injection molding is considered and then compared to the original model (2). The rate-of-deformation tensor \mathbf{D} corresponding to these two flows is

respectively given by

$$\mathbf{D}_1 = \frac{1}{2} \begin{bmatrix} 0 & 0 & \dot{\gamma} \\ 0 & 0 & 0 \\ \dot{\gamma} & 0 & 0 \end{bmatrix}, \quad \mathbf{D}_2 = \begin{bmatrix} 1 & 0 & 0 \\ 0 & 0 & 0 \\ 0 & 0 & -1 \end{bmatrix} \dot{\epsilon}. \quad (5)$$

In the case of a simple shear in the 1-3 plane given by \mathbf{D}_1 in (5), a direct application of (4) along with the stress expression (2) by replacing the 4th-order viscosity \mathbb{V} by its scalar approximation η_* gives

$$\mathbf{a}_* = 2\mathbb{A}_{1313} \implies \boldsymbol{\sigma}_* = \begin{bmatrix} -p & 0 & (1 + 2N_p\mathbb{A}_{1313})\eta\dot{\gamma} \\ 0 & -p & 0 \\ (1 + 2N_p\mathbb{A}_{1313})\eta\dot{\gamma} & 0 & -p \end{bmatrix}. \quad (6)$$

It can be seen that the most adequate scalar value of the 4th-order fiber orientation tensor for simple shear flows according to (4) is its component in the shear plane. Comparing the approximated stress tensor (6) to the original one given by (1), one finds that

- The 13 stress component is exactly the same. The shear viscosity is thus given by

$$\eta_s = \sigma_{13}/\dot{\gamma} = (1 + 2N_p\mathbb{A}_{1313})\eta \quad (7)$$

for both the original and optimal scalar models.

- However as expected the approximate model does not present any normal stress differences, while for the original one we have for instance

$$N_1 = \sigma_{11} - \sigma_{22} = 2N_p(\mathbb{A}_{1113} - \mathbb{A}_{2213})\eta\dot{\gamma}.$$

As for planar extensional flows given by \mathbf{D}_2 in (5), it can also be easily shown that the planar extensional viscosity (see [Petrie \(2006\)](#)) is exactly recovered during the scalar approximation process (4), which is given by

$$\eta_p = \frac{\sigma_{11} - \sigma_{33}}{\dot{\epsilon}} = 2(2 + N_p\mathbb{A}_{1111} - 2N_p\mathbb{A}_{1133} + N_p\mathbb{A}_{3333})\eta = 4(1 + N_p\mathbf{a}_*)\eta. \quad (8)$$

One can check that when fiber contributions are small whenever N_p or \mathbb{A}_{ijkl} are, one retrieves the theoretical value $\eta_p = 4\eta$ for a Newtonian fluid, cf. [Petrie \(2006\)](#).

As an illustration of the fiber orientation effects present in the optimal scalar model (4), we consider two particular orientation states: a fully random state \mathbf{a}_R and a quasi-perfect unidirectional orientation one \mathbf{a}_{UD} . The 2nd-order fiber orientation tensors are respectively given by

$$\mathbf{a}_R = \frac{1}{3}\mathbf{I} = \frac{1}{3} \begin{bmatrix} 1 & & \\ & 1 & \\ & & 1 \end{bmatrix}, \quad \mathbf{a}_{UD} = \begin{bmatrix} \bar{a}_{11} & & \\ & \frac{1}{2}(1 - \bar{a}_{11}) & \\ & & \frac{1}{2}(1 - \bar{a}_{11}) \end{bmatrix} \quad (9)$$

with $\bar{a}_{11} = 0.98$. In [Fig. 3](#), the values of the coupling factor \mathbf{a}_* for these two particular orientation states under two typical flows (5) are indicated. We can see that

- Under simple shear, the coupling factor, and hence also the shear viscosity according to (6), are larger for the random orientation state than the unidirectional one. In the latter case the fiber contribution is negligible.
- For the planar extension case, fibers contribute the most to the planar extensional viscosity (8) when they are aligned with the extension direction. Their contribution is reduced when they are randomly oriented in space.

These theoretical observations are well conforming to the experimental findings presented for instance in [Laun \(1984\)](#).

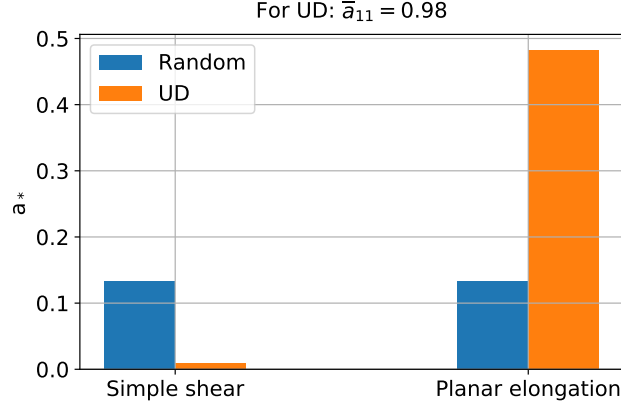


Figure 3: Coupling factor \bar{a}_* for two particular orientation states under two typical flows.

2.3. Implementation in the Moldflow Insight API framework

We recall that in (4), the viscosity η refers to that of the matrix in absence of fibers. In Moldflow API simulations, it is more convenient to still select the fiber reinforced material (say 50%wt) with a measured viscosity η_{MF} , based on which we will then apply a scaling factor $\hat{\eta}$ incorporating anisotropic effects according to (4). Consequently, we need to recover from η_{MF} at least approximately the viscosity function η corresponding to the non-filled matrix. Since in Moldflow the apparent viscosity η_{MF} is measured using a capillary rheometer at relatively high shear rates, the fibers should be almost perfectly aligned in the shear direction, see [Costa et al. \(2015\)](#). We consider hence a simple shear flow $\mathbf{v} = x_3\dot{\gamma}\mathbf{e}_1$ in the 1-3 plane where the deformation rate is given by \mathbf{D}_1 in (5). Due to possible fiber-fiber/matrix interactions (see [Folgar and Tucker \(1984\)](#) for instance), the alignment is not perfect and we suppose that the 2nd order fiber orientation tensor can be parametrized by its 11 component and is given by \mathbf{a}_{UD} in (9), where \bar{a}_{11} should be in general very close to 1 characterizing a quasi unidirectional state. Applying our optimal scalar viscosity (4) for \mathbf{a}_{UD} under the simple shear flow gives

$$\eta_{MF} = (1 + N_p\bar{a}_*)\eta, \quad (10)$$

where \bar{a}_* is obtained by combining (4) with \mathbf{a}_{UD} in (9) and \mathbf{D}_1 in (5)

$$\bar{a}_* = \frac{\mathbf{D}_1 \cdot \mathbb{A}\mathbf{D}_1}{\|\mathbf{D}_1\|^2}, \quad \mathbb{A} = \mathbb{A}(\mathbf{a}_{UD}(\bar{a}_{11})).$$

Its functional dependence with respect to \bar{a}_{11} is illustrated in [Fig. 4](#). We verify that for $\bar{a}_{11} = 1$ when the fibers are (somehow indeed) perfectly aligned in the shear direction, the Moldflow apparent viscosity η_{MF} directly gives the matrix viscosity η since in this case fibers have no effect on the suspension viscosity, resulting in $\bar{a}_* = 0$. For other cases, this small coefficient \bar{a}_* reflects thus the fiber alignment information contained in the Moldflow fiber reinforced suspension viscosity. Two particular values of \bar{a}_{11} that will be used in the following numerical simulations in [Section 3](#) are also indicated in [Fig. 4](#).

Combining (4) et (10), we finally obtain the optimal scalar fiber-induced rheological model that will be implemented in the Moldflow API framework

$$\eta_*(\mathbf{D}, T, p, \mathbf{a}) = \hat{\eta}(\mathbf{D}, \mathbf{a}) \cdot \eta_{MF}(\dot{\gamma}, T, p) = \frac{1 + N_p\mathbf{a}_*(\mathbf{D}, \mathbf{a})}{1 + N_p\bar{a}_*} \eta_{MF}(\dot{\gamma}, T, p). \quad (11)$$

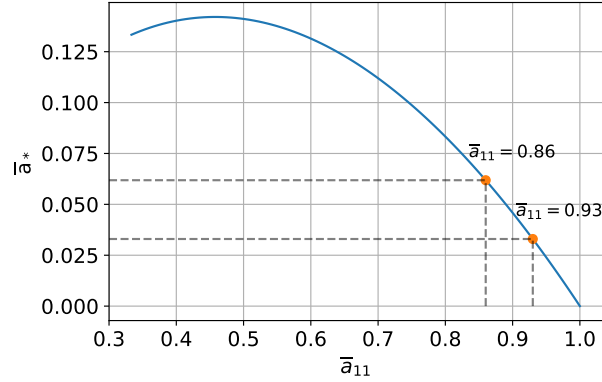


Figure 4: Variation of \bar{a}_* as \bar{a}_{11} increases from $1/3$ (isotropic state) to 1 (unidirectional state).

We recall that here $\hat{\eta}$ is the non-dimensional viscosity scaling factor that will be applied to the Moldflow fiber reinforced suspension viscosity η_{MF} . Observe that now the shear rate (tensor) dependence of the resulting semi-anisotropic fiber dependent viscosity η_* is both through the original Moldflow viscosity function (mainly the Cross model) and the coefficient \bar{a}_* adapting fiber orientation \mathbf{a} induced anisotropy to the current deformation rate tensor \mathbf{D} via (4). The temperature T and pressure p dependence remain unchanged compared to standard uncoupled simulations.

3. Test-case simulations on a rectangle plate

In this section we intend to investigate numerically the effect of fiber-induced viscosity models presented in Section 2 through injection molding simulations under Autodesk Moldflow. The version Moldflow Insight 2018 is used.

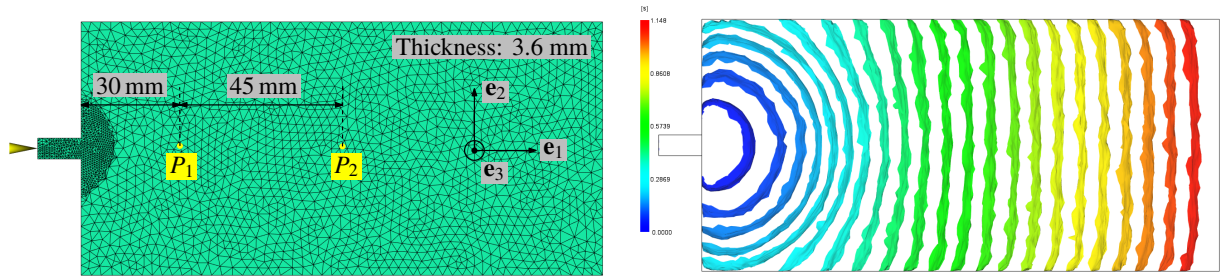


Figure 5: (Left) Rectangle end-gated flat plate with two probe points as used in Costa et al. (2015); (right) Filling contour for uncoupled injection simulations.

The Moldflow study (.sdy) file is kindly provided by the first author of Costa et al. (2015) and we use the same geometry, basic material, injection process and numerical parameters as used in Costa et al. (2015). As can be seen from Fig. 5 (left), the geometry consists of a simple end-gated rectangle flat plate with a thickness of 3.6 mm. Two probe points P1 (upstream, near the gate) and P2 (downstream, at the plate center) are used to analyze the simulation. The default material parameters of a 50%wt fiber filled polyamide (Zytel PLS95G50DH2 BK261) in the Moldflow database are used, with a standard Cross-WLF viscosity model. The Phan-Thien and Graham (1991)'s N_p parameter is computed using the aspect ratio and volume fraction information contained in the Moldflow database, and a fitting parameter $A = 50\%$, which

gives $N_p \approx 221$ (see also Fig. 1). Since we are mainly interested in the coupling between flow equations and fiber orientations, only a filling simulation without packing phase can be considered. For comparison concerns we fix a constant ram speed at 50 mm/s which leads to an injection time near 1.15 s. The spatial discretization is realized with sufficiently fine triangles on the surfaces and 16 layers of tetrahedral elements in the gapwise direction.

It will be interesting to evaluate the flow-fiber coupling effects introduced by the fiber-induced viscosity models presented in Section 2, for several fiber orientation models which may contribute differently to the overall coupling. In this communication we will use the two principal fiber orientation models available in Moldflow Insight 2018: the Reduced Strain Closure (RSC) model proposed by Wang et al. (2008) and the lately introduced Moldflow Rotational Diffusion (MRD) model (see Autodesk (2016)). Note that since the Moldflow version 2017R2, the default fiber orientation model becomes the MRD model.

3.1. Fiber orientations predicted by the RSC and MRD models

We will first compare these two fiber orientation models using the default uncoupled viscosity model (Cross-WLF). The default parameters for these fiber models are used. Since the flow equations and the fiber orientation model are uncoupled, the same filling pattern is obtained as illustrated in Fig. 5 (right). Contrary to the experimental results indicated in Costa et al. (2015) where the flow advances faster near the edge than in the center, the simulated contours are essentially convex throughout the filling phase.

The steady a_{11} and a_{13} fiber orientation components in the thickness direction of the probe point P1 are presented in Fig. 6 for both models. At P2 similar results can be obtained and hence are not illustrated here. We recall that the 1-axis corresponds to the horizontal flow direction while the 3-axis is the thickness one, see Fig. 5 (left). The thickness coordinate z is normalized such that -1 (resp. +1) corresponds to the lower (resp. upper) surface and 0 designates the mid-surface. As for the a_{11} component, the well-known skin-shell-core structure can be observed for both fiber models, though the RSC model predicts a more flow-aligned orientation in the shear-dominated shell region. It is also interesting to see that the RSC model gives a larger (yet still small) a_{13} component especially in the shell and skin regions. Note that the trend reported here in Fig. 6 should not be general and only reflects the default parameters set in Moldflow.

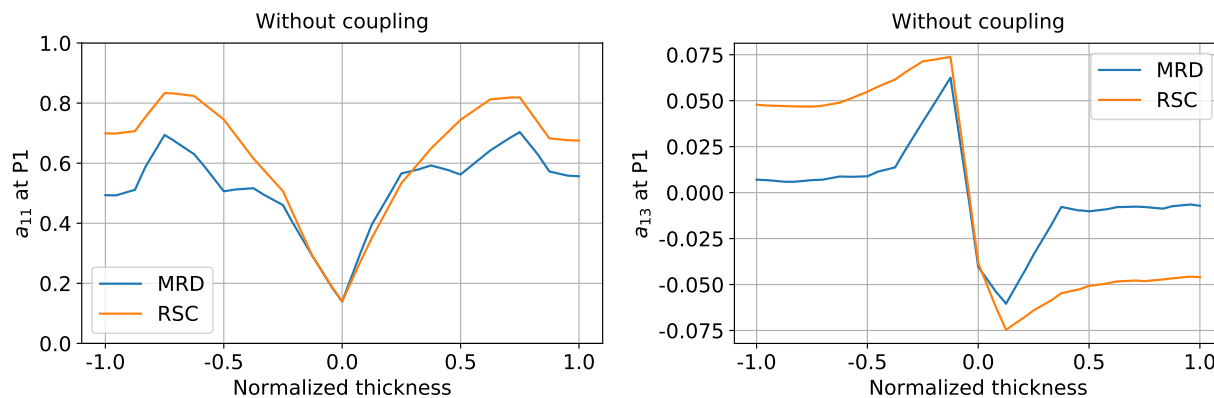


Figure 6: Fiber orientation a_{11} (left) and a_{13} (right) components at P1 for both MRD and RSC models without viscosity coupling effects.

3.2. Coupled simulations using the MRD fiber model

We first test the optimal scalar fiber-induced rheological model (11) using the MRD fiber model. The a_{11} variation in the thickness for both probe points are presented in Fig. 7. At P1, the flow-fiber coupled

model predicts a widened fiber core region compared to the uncoupled case due to the flow-fiber coupling. It also shows a slightly more orientated shell region. At P2, fibers are somehow predicted to be more aligned in the flow direction compared to the uncoupled model. Nevertheless the fiber orientation still displays a plausible skin-shell-core structure.

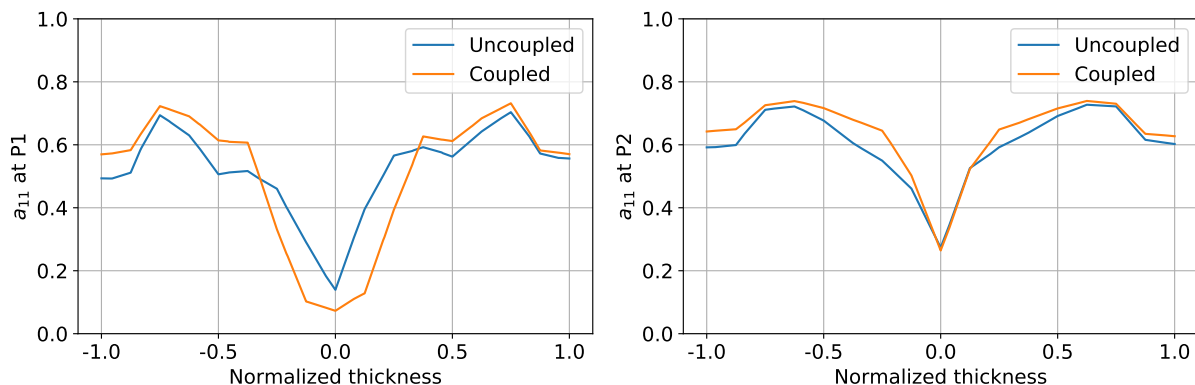


Figure 7: Fiber orientation a_{11} component at P1 (left) and P2 (right) probe points with the MRD model for the flow-fiber coupled model with $\bar{a}_{11} = 0.93$.

The velocity profile and viscosity at P1 are then analyzed in Fig. 8 to evaluate the effect of flow-fiber coupling on kinematics and rheological properties. It can be seen from Fig. 8 (left) that compared to the uncoupled case, the velocity profile is now essentially flattened (plug flow) in the core region resulting from the corresponding viscosity increase (by a factor of 10 at the center) as indicated in Fig. 8 (right). The overall deformation rate is thus significantly reduced in that region, which explains a less aligned core in Fig. 7 (left). Since the probe point P1 is near the gate, we suspect that this fiber-induced increased viscosity should originate from an elongational flow in the transverse direction. This point will be verified in the next section.

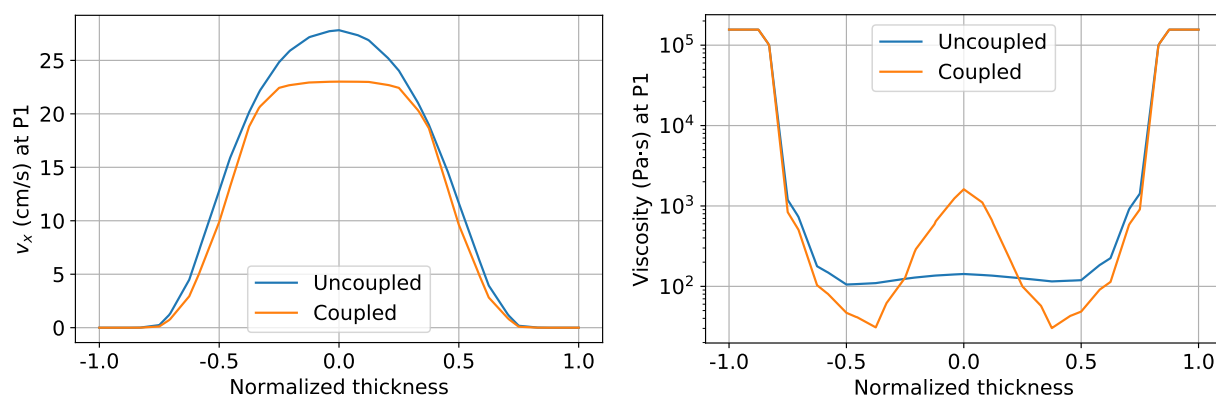


Figure 8: Results obtained at the end of filling at P1 with the MRD model for the flow-fiber coupled model with $\bar{a}_{11} = 0.93$: (Left) Velocity profile v_x ; (Right) Viscosity profile.

Concerning the overall filling pattern when using the flow-fiber coupled model (11), it is essentially the same as that illustrated in Fig. 5 for the uncoupled case. As in Costa et al. (2015), the viscosity increase only concerns a limited core region (according to Fig. 8 (right), only about 25% of the thickness). That's probably why here it fails to predict a locally concave contour as shown in Costa et al. (2015).

3.3. Coupled simulations with the RSC model

Now the flow-fiber coupling effects introduced by (11) will be evaluated for the RSC model. Again we first compare the fiber orientation profile at both probe points for the coupled and uncoupled cases. For the \bar{a}_{11} parameter characterizing fiber alignment in the Moldflow viscosity (see Fig. 4), two values are tested. According to Fig. 9, fiber orientation is not very sensitive to the \bar{a}_{11} parameter. Interestingly, compared to the MRD case (Fig. 7), now for both probe points we have a slowed down fiber alignment throughout the thickness and consequently a widened fiber core region. This indicates that different fiber models may also contribute differently to the overall coupling effect.

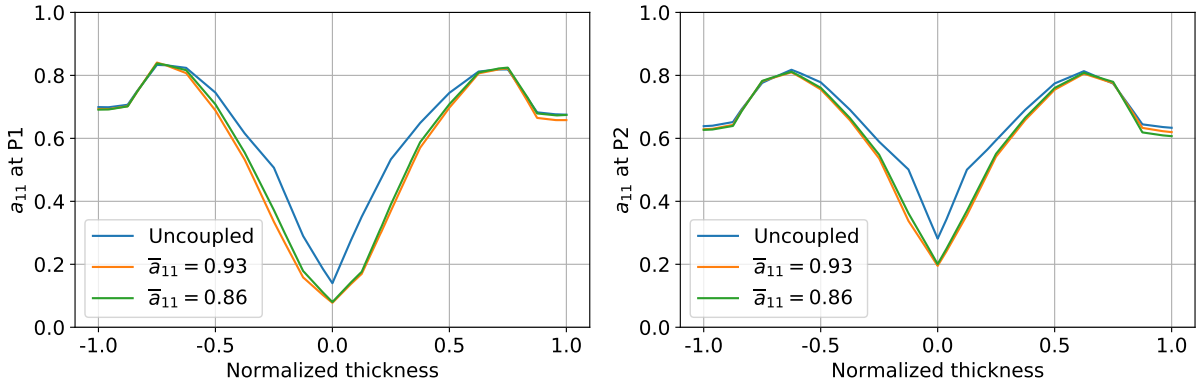


Figure 9: Fiber orientation a_{11} at P1 (left) and P2 (right) with the RSC model for the flow-fiber coupled model.

In Figs. 7 and 9, only the final fiber orientation states at the end of filling are presented. It will also be interesting to analyze temporal fiber evolutions for both coupled and uncoupled models. The averaged (in the thickness direction) fiber orientation as a function of filling time is illustrated in Fig. 10. It can be observed that the temporal fiber orientation increases monotonically. Due to flow-induced viscosity increase, the overall deformation rate is reduced implying a systematic slowed down fiber alignment.

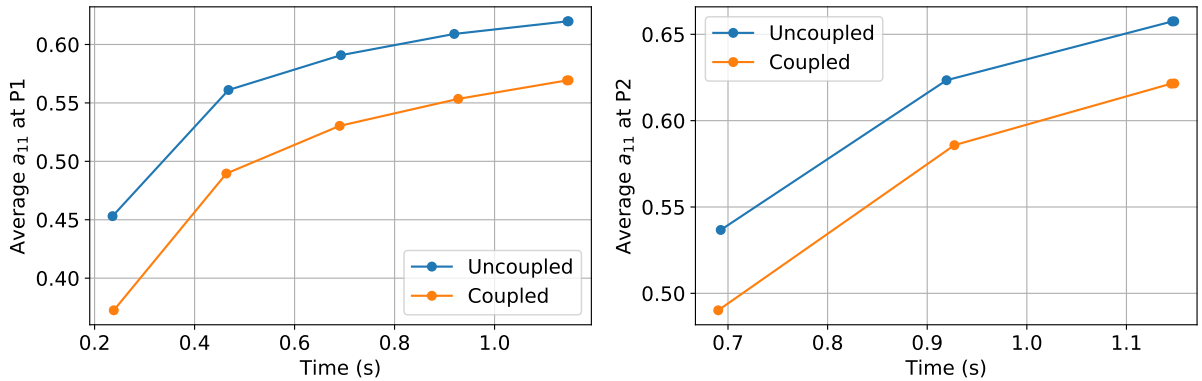


Figure 10: Temporal evolution of the average a_{11} in the thickness at P1 (left) and P2 (right) with the RSC model for the flow-fiber coupled model $\bar{a}_{11} = 0.86$.

Now, we will investigate what exactly happened at these two probe points P1 and P2 that leads to what we observe in Figs. 7 to 10. For that, we need to analyze the deformation rate tensor \mathbf{D} in the thickness direction. Since the tensor components of \mathbf{D} are not directly available in Moldflow, the velocity field \mathbf{v} at the end of fill is exported through a home-made script to another post-processing software, where the gradient

of \mathbf{v} can be automatically computed. To make sure that our computation of $\mathbf{D} = \frac{1}{2} \text{dev}(\nabla\mathbf{v} + \nabla^T\mathbf{v})$ matches that of Moldflow, the generalized shear rate $\dot{\gamma} = \sqrt{2} \|\mathbf{D}\|$ is first compared in Fig. 11. The shear rate given by Moldflow can be indeed accurately recovered, which validates our post-processing approach. The small discrepancy mainly originate from different interpolation schemes of the velocity and averaging processes.

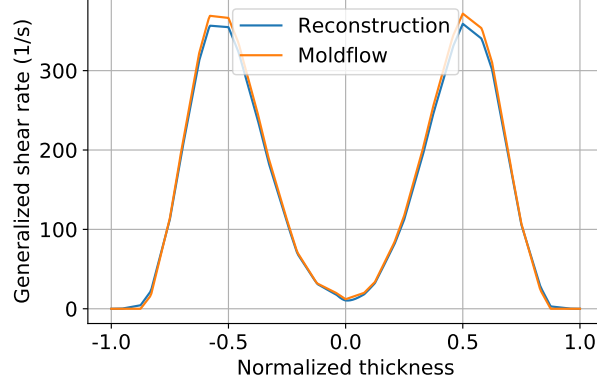


Figure 11: Reconstruction of the generalized scalar shear rate at P1.

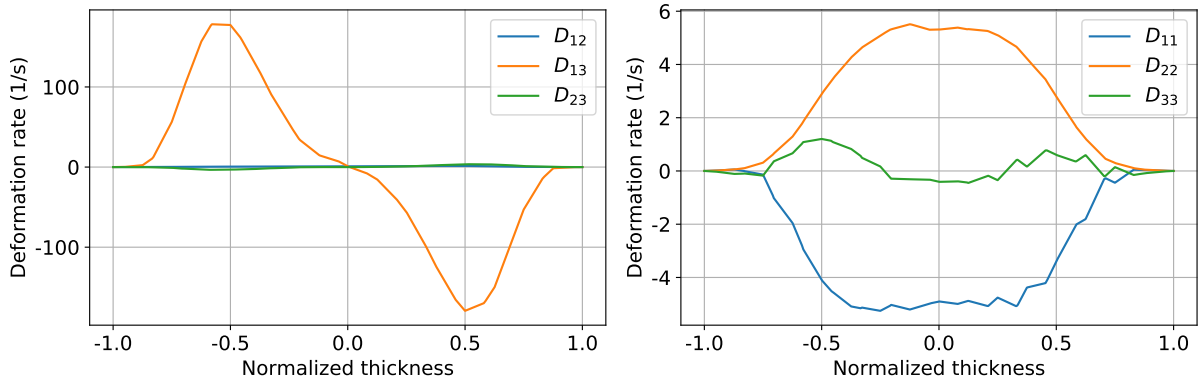


Figure 12: Deformation rate at P1 with the RSC model for the flow-fiber coupled model at $\bar{a}_{11} = 0.93$: (left) shear components and (right) elongational components.

It can be seen from Fig. 12 (left) that the 13 shear component is dominant compared to other shear components, which is fairly typical for thin-walled injection molding, see Tucker (1991). According to Fig. 12 (right), a planar elongational flow toward the transverse direction is indeed observed especially on the mid-surface $z = 0$ at P1, where the deformation rate tensor is given by

$$\mathbf{D} = \begin{bmatrix} -4.9 & 0.8 & 0.9 \\ 0.8 & 5.3 & 0 \\ 0.9 & 0 & -0.4 \end{bmatrix} 1/\text{s}.$$

Using the reconstructed deformation rate tensor in Fig. 12 and the fiber orientation tensors in Fig. 9 (left), the analytical formula of the optimal scalar flow-fiber coupled model (11) can be applied. The thus obtained theoretic viscosity scaling factor is compared to Moldflow results in Fig. 14 (left). A relatively good agreement can be found between them, which hence validates our implementation of (11) in the Moldflow Insight API framework. Again, the slight discrepancy may mainly originate from the exact calculation of

the deformation tensor and especially different averaging operators in Moldflow and our post-processing. At the mid-surface a viscosity scaling factor near 10 is retrieved (see Fig. 8). This illustrates that it is indeed the planar extensional flow in the 2 direction together with a nearly transverse fiber orientation state in the core region as shown in Fig. 9 that are mainly responsible for the viscosity increase in the core region, conforming to our previous theoretical analysis in Fig. 3.

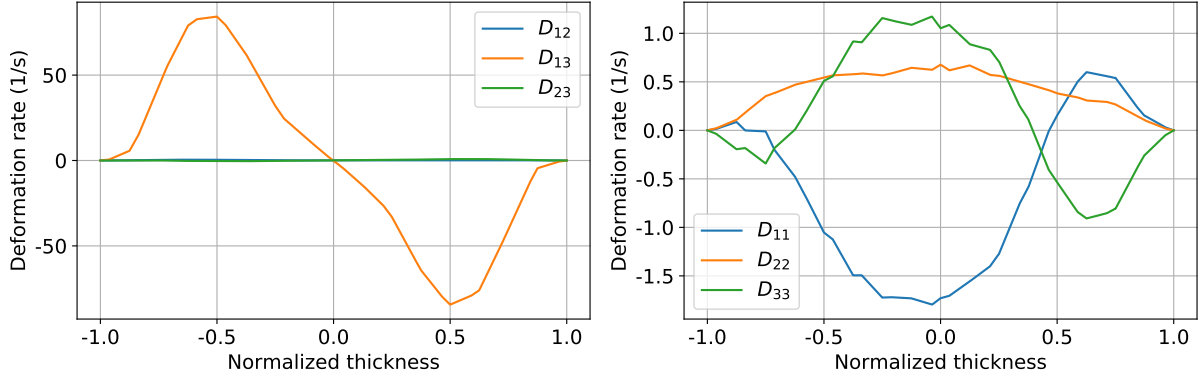


Figure 13: Deformation rate at P2 with the RSC model for the flow-fiber coupled model at $\bar{a}_{11} = 0.93$: (left) shear components and (right) elongational components.

The above analyses are now applied to the probe point P2 in Fig. 13. This time the deformation rate tensor at the mid-surface is now given by

$$\mathbf{D} = \begin{bmatrix} -1.7 & 0.1 & -0.2 \\ 0.1 & 0.7 & 0.1 \\ -0.2 & 0.1 & 1.1 \end{bmatrix} 1/\text{s}.$$

It can be observed that at the downstream point P2 we no longer have a planar divergent flow but a biaxial extensional flow toward the 2-3 directions in the core region. Furthermore, in terms of magnitude it is also not comparable to that observed at the upstream probe point P1, which is fairly typical for rectangle end-gated plates. It must be something else that contributes primarily to a widened fiber orientation core observed in the RSC model at P2, see Fig. 9 (right). In Fig. 14 (right), we compare the viscosity scaling factor obtained with the MRD and the RSC model. Although at the mid-surface the MRD gives a slightly larger value, the RSC model presents a larger overall value in the whole thickness. Since the 13 shear component is dominant almost throughout the thickness except very near the mid-surface, the flow-fiber coupling should mainly come from the fibers oriented in that plane. According to Fig. 6 (right), by default the RSC model predicts indeed more fiber orientations in the 13 plane than the MRD model. In the authors' opinion this maintains the overall viscosity in the shell region with the RSC model, and in the same time widens the core region in Fig. 9 (right) due to a scaling factor still larger than 1 in the core gion.

Finally, in Fig. 15, we compare the pressure temporal evolution at the injection point, for two values of \bar{a}_{11} . A larger value (closer to 1) of \bar{a}_{11} leads to an overestimated evolution compared to the uncoupled case. This agrees well with our definition in (10) since in the limiting case $\bar{a}_{11} = 1$, we have $\bar{a}_* = 0$ and the uncoupled Moldflow viscosity is assumed to be that of the unfilled matrix, based on which we will apply then a scaling factor $1 + N_p \bar{a}_*$ always bigger than 1. This may very likely increase the overall pressure prediction. The use of a smaller \bar{a}_{11} assumes that fibers are not perfectly aligned during the Moldflow measurement of viscosity, and compensates the pressure prediction. This parameter \bar{a}_{11} can thus be regarded as a fitting parameter of the model.

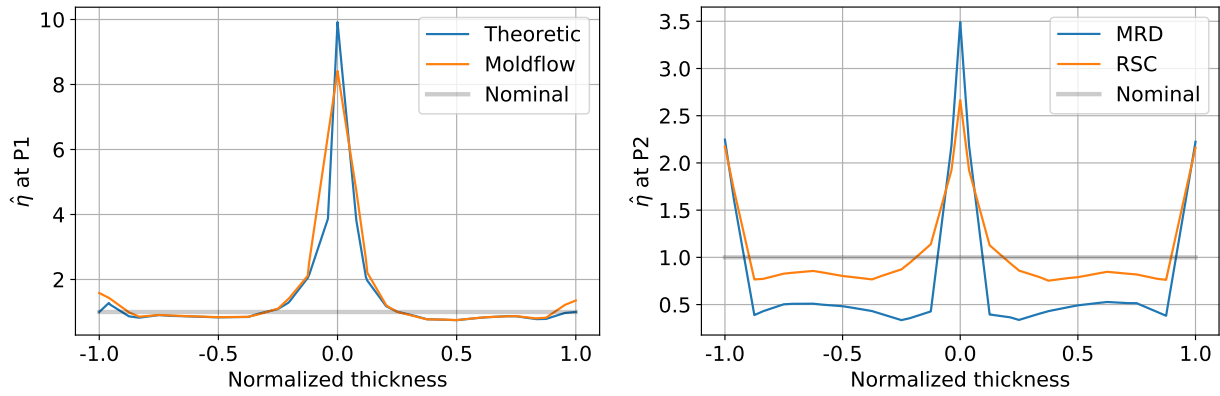


Figure 14: Viscosity scaling factor for the optimal scalar flow-fiber coupled model at $\bar{a}_{11} = 0.93$: (left) comparison at P1 between theoretic and Moldflow values with the RSC model; (right) comparison between the MRD and RSC fiber models at P2 (Moldflow calculations)

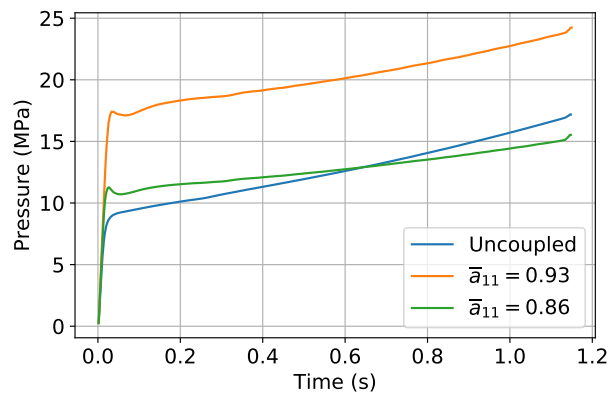


Figure 15: Pressure at the injection point with the RSC model for the flow-fiber coupled model.

4. Conclusions and future work

From rheological modeling of fiber-reinforced suspension point of view, this paper proposed a modified yet *optimal* version (4) of the original viscosity model that reduces an anisotropic 4th order tensor to a scalar, even though it was initially motivated by computational implementation purposes. According to our preliminary theoretic analyses in Section 2.2 and coupled simulation results presented in Section 3, the optimal scalar model (4) performs equally well compared to the original one and successfully captures elongational flows and fiber orientation components in the dominating shear plane.

Via these fiber-dependent viscosity models, flow kinematics and fiber evolutions are now tightly two-way coupled through rheological properties. In particular, a slowed down fiber alignment in the flow direction with a widened core region can be obtained, depending directly on the particular local deformation conditions and fiber states. Using the optimal scalar flow-fiber coupled model (4), it is expected that the extensional flows will be better taken into account especially in the core region. Fiber orientation prediction for geometrically complex chunky parts Kleindel et al. (2015) could be improved.

In this paper, the flow-fiber coupling effects are evaluated by two latest fiber orientation models available in Moldflow. Since once established the coupling works both ways, different fiber models may deliver different contributions to overall flow-fiber coupling. Attention must be taken when comparing results of coupled simulations with different orientation models. According to our results in Section 3, it seems that the RSC model results in more coupling effects than the newly introduced MRD model. Note that this conclusion may only be limited to the behaviors using default parameters.

This paper reports some of the preliminary results of our research on fiber-induced viscosity modeling. It will be followed by additional communications that may include the following interesting theoretical and practical aspects:

- Comprehensive theoretic rheological analyses and computational details of the optimal scalar viscosity model (4): further comparison with the original model in terms of approximation errors, implementation technicalities in the Moldflow Insight API framework, computational efficiency¹...
- Accounting for other additional fiber-induced rheological contributions. Different coupling may exist between flow equations and fiber evolution models, as indicated in Fig. 16. In this paper only orientation effects are considered. Future work could be for instance devoted to the coupling effects introduced by a non-homogeneous volume fraction distribution, which itself is predicted by a fiber migration model such as Morris (2009).

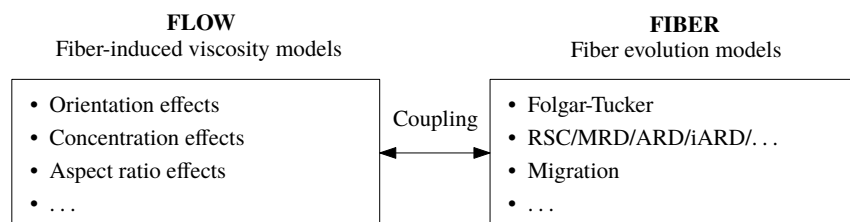


Figure 16: Coupling between flow equations and fibers through fiber-induced viscosity models.

¹Contrary to what may have been suggested in Kleindel et al. (2015), coupled injection simulations are not so costly according to our experiences.

- Implications of coupled injection molding simulations in subsequent integrative mechanical simulations that take into account the previous processing results: how the stress distribution is varied by using a fiber-flow coupling injection simulation;
- Experimental validation of the proposed flow-fiber coupled simulations on structural parts.

Acknowledgement

The work presented in this document is financially supported by the [THERMOFIP](#) research program coordinated by Solvay Engineering Plastics. The authors would like to express again their sincere gratitude to Autodesk Moldflow developers and in particular Dr. Franco Costa for his guidance and valuable comments. Also, the Moldflow API simulations presented in [Section 3](#) can not be performed without the kind and generous help of Alain Benchissou from APLICIT.

Competing interests

The authors declare that they have no competing interests.

References

- Adam, L., Assaker, R., 2014. Integrated nonlinear multi-scale material modelling of fiber reinforced plastics with Digimat: Application to short and continuous fiber composites. In: Proceedings of the 11th World Congress on Computational Mechanics. pp. 20–25.
- Advani, S. G., Tucker, C. L., 1987. The use of tensors to describe and predict fiber orientation in short fiber composites. *Journal of Rheology* 31 (8), 751–784.
- Autodesk, 2016. Fiber Orientation Accuracy Validation Report of Moldflow Insight 2017 R2.
- Cintra Jr, J. S., Tucker, C. L., 1995. Orthotropic closure approximations for flow-induced fiber orientation. *Journal of Rheology* 39 (6), 1095–1122.
- Costa, F., Cook, P., Pickett, D., 2015. A framework for viscosity model research in injection molding simulation, including pressure and fiber orientation dependence. In: SPE ANTEC Conference.
- Ericksen, J. L., 1959. Anisotropic fluids. *Archive for Rational Mechanics and Analysis* 4 (1), 231.
- Folgar, F., Tucker, C. L., 1984. Orientation behavior of fibers in concentrated suspensions. *Journal of Reinforced Plastics and Composites* 3 (2), 98–119.
- Jørgensen, J. K., Andreassen, E., Salaberger, D., 2017. The effect of fiber concentration on fiber orientation in injection molded film gated rectangular plates. *Polymer Composites*.
- Kleindel, S., Salaberger, D., Eder, R., Schretter, H., Hochenauer, C., 2015. Prediction and validation of short fiber orientation in a complex injection molded part with chunky geometry. *International Polymer Processing* 30 (3), 366–380.
- Laun, H. M., 1984. Orientation effects and rheology of short glass fiber-reinforced thermoplastics. *Colloid & Polymer Science* 262 (4), 257–269.
- Lipscomb, G. G., Denn, M. M., Hur, D. U., Boger, D. V., 1988. The flow of fiber suspensions in complex geometries. *Journal of Non-Newtonian Fluid Mechanics* 26 (3), 297–325.
- Mazahir, S., Vélez-García, G., Wapperom, P., Baird, D., 2013. Evolution of fibre orientation in radial direction in a center-gated disk: Experiments and simulation. *Composites Part A: Applied Science and Manufacturing* 51, 108–117.
- Morris, J. F., 2009. A review of microstructure in concentrated suspensions and its implications for rheology and bulk flow. *Rheologica acta* 48 (8), 909–923.
- Papathanasiou, T. D., 1997. Flow-induced alignment in composite materials. Woodhead Publishing Cambridge, Ch. Flow-induced alignment in injection molding of fiber-reinforced polymer composites.
- Petrie, C. J. S., 2006. Extensional viscosity: A critical discussion. *Journal of Non-Newtonian Fluid Mechanics* 137 (1), 15–23.
- Phan-Thien, N., Graham, A., 1991. A new constitutive model for fibre suspensions: flow past a sphere. *Rheologica acta* 30 (1), 44–57.
- Phan-Thien, N., Zheng, R., 1997. Flow-induced alignment in composite materials. Woodhead Publishing Cambridge, Ch. Macroscopic modelling of the evolution of a fibre orientation during flow.

- Ranganathan, S., Advani, S. G., 1993. A simultaneous solution for flow and fiber orientation in axisymmetric diverging radial flow. *Journal of Non-Newtonian Fluid Mechanics* 47, 107–136.
- Redjeb, R., Silva, L., Laure, P., Vincent, M., Coupez, T., 2006. Three dimensional numerical simulations of fiber orientation in injection molding. In: 9th ESAFORM.
- Rolland, H., Saintier, N., Robert, G., 2016. Damage mechanisms in short glass fibre reinforced thermoplastic during in situ microtomography tensile tests. *Composites Part B: Engineering* 90, 365–377.
- Tseng, H.-C., Chang, R.-Y., Hsu, C.-H., 2017. Improved fiber orientation predictions for injection molded fiber composites. *Composites Part A: Applied Science and Manufacturing* 99, 65–75.
- Tucker, C. L., 1991. Flow regimes for fiber suspensions in narrow gaps. *Journal of Non-Newtonian Fluid Mechanics* 39 (3), 239–268.
- Verweyst, B. E., 1998. Numerical predictions of flow-induced fiber orientation in three-dimensional geometries. Ph.D. thesis, University of Illinois at Urbana-Champaign.
- Verweyst, B. E., Tucker, C. L., 2002. Fiber suspensions in complex geometries: Flow/orientation coupling. *The Canadian Journal of Chemical Engineering* 80 (6), 1093–1106.
- Vincent, M., Giroud, T., Clarke, A., Eberhardt, C., 2005. Description and modeling of fiber orientation in injection molding of fiber reinforced thermoplastics. *Polymer* 46 (17), 6719–6725.
- Wang, J., O’Gara, J. F., Tucker, C. L., III, 2008. An objective model for slow orientation kinetics in concentrated fiber suspensions: Theory and rheological evidence. *Journal of Rheology* 52 (5), 1179–1200.
- Wedgewood, A., Zhang, Z., Sulmoni, M., Kang, S., 2017. Addressing practical challenges in developing Digimat material laws. In: Digimat Users’ Meeting, Berlin, Germany.